Journal of Material Cycles and Waste Management

Thermal decomposition of cement-asbestos at 1100 °C: how much “safe” is “safe”?

--Manuscript Draft--

Manuscript Number:	JMCW-D-21-00684
Full Title:	Thermal decomposition of cement-asbestos at 1100 °C: how much “safe” is “safe”?
Article Type:	Original Article
Corresponding Author:	Giancarlo Capitani University of Milano–Bicocca: Universita degli Studi di Milano-Bicocca ITALY
Corresponding Author Secondary Information:	
Corresponding Author's Institution:	University of Milano–Bicocca: Universita degli Studi di Milano-Bicocca
Corresponding Author's Secondary Institution:	
First Author:	Fabrizio Vergani
First Author Secondary Information:	
Order of Authors:	Fabrizio Vergani
	Lucia Galimberti
	Mihaela Narcisa Marian
	Giovanna Giorgetti
	Cecilia Viti
	Giancarlo Capitani
Order of Authors Secondary Information:	
Funding Information:	Italian Ministry for the Ecologic Transition (SNSvS, NP 2.7, DEAR: deattivazione efficiente dell'amianto e riutilizzo) — Prof. Giancarlo Capitani
Abstract:	The products of cement-asbestos treated in air at 1100 °C were characterized by a multimethodological approach, to determine 1) the effective deactivation of harmful asbestos fibers; 2) the mineralogy and microstructure of the inert product and its possible use as a secondary raw material (SRM); and 3) any potential health hazard of the SRM. For this purpose, energy dispersive X-ray fluorescence spectrometry (EDXRF), X-ray powder diffraction (XRPD), scanning, and transmission electron microscopy (SEM and TEM) analyses were performed. The powdered SRM was also analyzed by dynamic laser scattering and solution leaching experiments, to determine grain size distribution and possible elements release. Our results confirm the deactivation of crocidolite and chrysotile asbestos fibers, but at the same time evidence a significant fraction of nanoparticles in the SRM and some critical releases of SO_4^{2-}, F^- and Cr^{6+} in solution. Both the nanoparticle fraction and the critical elemental release may pose human health concern and adversely effect on potential applications of the SRM. Strategies to control the grain size distribution through adjusted thermal treatment conditions and microwave assisted grinding operations are discussed. Possible routes to safely reuse the SRM are indicated.
Suggested Reviewers:	Girolamo Belardi CNR Italy girolamo.belardi@cnr.it expert of similar topics
	Paolo Plescia CNR Italy paolo.plescia@cnr.it expert of similar topics

	Danilo Spasiano University of Bari: Universita degli Studi di Bari Aldo Moro danilo.spasiano@uniba.it expert of similar topics
	Enrico Bernardo University of Padova: Universita degli Studi di Padova enrico.bernardo@unipd.it expert of similar topics
	Giovanni Valdrè University of Bologna: Universita di Bologna giovanni.valdre@unibo.it expert of similar topics

Thermal decomposition of cement-asbestos at 1100 °C: how much "safe" is "safe"?

Vergani F.[a], Galimberti L.[a], Marian N. M.[b], Giorgetti G.[b], Viti C.[b], Capitani G.C.[a]

[a] Department of Earth and Environmental Sciences (DISAT), University of Milano-Bicocca, Piazza della Scienza 4, I-20126, Milano, Italy

[b] Department of Physical Science, Earth and Environment (DSFTA), University of Siena, V. Laterina 8, I-53100, Siena, Italy

Corresponding author: Capitani Giancarlo, giancarlo.capitani@unimib.it

Abstract

The products of cement-asbestos treated in air at 1100 °C were characterized by a multimethodological approach, to determine 1) the effective deactivation of harmful asbestos fibers; 2) the mineralogy and microstructure of the inert product and its possible use as a secondary raw material (SRM); and 3) any potential health hazard of the SRM. For this purpose, energy dispersive X-ray fluorescence spectrometry (EDXRF), X-ray powder diffraction (XRPD), scanning, and transmission electron microscopy (SEM and TEM) analyses were performed. The powdered SRM was also analyzed by dynamic laser scattering and solution leaching experiments, to determine grain size distribution and possible elements release. Our results confirm the deactivation of crocidolite and chrysotile asbestos fibers, but at the same time evidence a significant fraction of nanoparticles in the SRM and some critical releases of SO_4^{2-}, F^- and Cr^{6+} in solution. Both the nanoparticle fraction and the critical elemental release may pose human health concern and adversely effect on potential applications of the SRM. Strategies to control the grain size distribution through adjusted thermal treatment conditions and microwave assisted grinding operations are discussed. Possible routes to safely reuse the SRM are indicated.

Keywords

Cement-asbestos,

Thermal treatment,

Leaching test,

Nanoparticles,

Chrysotile,

Crocidolite

1. Introduction

In the past, asbestos minerals (chrysotile and five fibrous amphiboles, among which crocidolite) have been widely used in building materials, due to their extraordinary properties of mechanical, chemical, and thermal strength. Cement-asbestos, which is a composite material where asbestos fibers are added to a cement matrix, is among the most used asbestos containing material (ACM), especially in roofing slates and other building components. Most have been manufactured through the Hatschek process and its modifications: a very dilute slurry made up of a mix of asbestos fibers (up to 10–15 wt% of the total product) and ordinary Portland cement (OPC) was gradually dried, obtaining films of about 0.3 mm in thickness, which were wound up on a roll to a desired specific thickness, and finally shaped [1]. The acclaimed carcinogenicity of asbestos led to its international ban since the 1990s but, due to its extremely wide use in the past, ACM are still widespread worldwide. In Italy, for instance, after the asbestos ban by law 257/92 [2] and law 248/04 [3] regulating ACM management, the commonly adopted strategies are: i) in situ encapsulation; ii) in situ confinement and iii) removal and subsequent disposal in national or foreign controlled landfills. All the above solutions have some drawbacks. Encapsulation, usually consisting in the application of special resins on the ACM surface to avoid fiber environmental release, is typically subject to weathering and requires periodic maintenance. Confinement, that is the creation of a barrier between ACM and the nearby environment, may be subject to accidental damage, as in the case of careless maintenance operations, extreme natural phenomena, or terrorist attacks. Removal and disposal in controlled landfills also have several disadvantages: i) asbestos containing waste (ACW) continues to constitute an environmental hazard, since asbestos fibers could be released in air or in groundwater; ii) controlled landfilling of huge ACW volumes requires land consumptions; iii) the existent landfills are inadequate to host present and future ACW, at least in Italy [4]; iv) the realization of possible new sites for ACW landfilling is not easily accepted by the community. In compliance with EU Parliament Resolution of the 14th of March 2013 “On asbestos related occupational health threats and prospects for abolishing all existing asbestos” (2012/2065(INI)) [5], a smarter alternative to landfill disposal of ACW is represented by deactivation of the toxic fibers through physical, chemical or biological processes, followed by possible recycling of the deactivated ACW as a safe secondary raw material (SRM). Indeed, many processes have been proposed in recent years, but unfortunately disposal in controlled landfills continues to be the most adopted solution, being the most economically advantageous. The main drawbacks of most ACW inertization techniques proposed so far can be schematically summarized as follows: i) high energy consumption due to long-time thermal treatment, necessary to ensure the complete decomposition of asbestos minerals; ii) large amount of reagents necessary for the chemical processes; iii) low efficiency of ACW bioremediation [6].

Notwithstanding, some processes based on vitrification at high temperature (1565-1600 °C) with plasma gun [7-10] or Joule heating [11-12] have been applied at industrial scale, as in the case of the Inertam plasma treatment plant in

France and the GeoMelt® treatment plant in Japan, respectively. The vitrification encompasses many advantages, among which complete fiber deactivation, ACW volume reduction, reusability of the end-products, but it is extremely energy-consuming [12]. Vitrified ACW can be used for the production of glass ceramics without any mineral additive and glass ceramic stoneware by adding industrial clay [13]. Other processes based on thermal decomposition of asbestos fibers at relatively lower temperature (800-1200 °C) have been tested in pilot plants, as in the case of the CORDIAM process [14-15] and the KRY-AS process [16-17]. These processes, operating at lower temperature than those required for vitrification, are more sustainable, but still not economically competitive with respect to landfilling. A recent innovative process, based on fast thermal inertization with processing times down to 15-20 minutes (Tuccitto & Grillo, Italian patent UBIM 25588/17), may fill the gap between promising experimental results and industrial realization of the first ACW operative inertization plant in Italy [18].

One of the key features in the overall economic analysis of ACW deactivation costs/benefits, is the possible use of the inert material as a secondary raw material (SRM). In all the above thermal inertization processes, the inert end-product is similar to a Mg-rich pozzolanic clinker – the magnesium content mostly inherited from the high-temperature degradation of asbestos minerals – thus potentially re-usable in the ceramic and cement industry [17, 19-22]. However, the treated product shows an extremely high degree of recrystallization of the original asbestos, inert and ligand phases into secondary crystalline phases and glass, with a grain size that spans from tens of microns to nanometers. In most cases, the treated material is relatively cohesive and self-sustaining, so that its possible industrial reuse would require a milling pre-treatment to get the necessary grain size. The final grain size of the SRM, that depends on thermal inertization details and subsequent milling procedures, is a key feature for both the efficacy and the competitiveness of the SRM, as well as for possible health concerns.

In this paper, we analyzed deactivated cement-asbestos (CA) slates after treatment in air at 1100 °C, focusing on the inert end-product mineralogical and microstructural characteristics, and on its possible safe re-use as a SRM in ceramic industries.

2. Material and methods

2.1. ACW collection and inertization

The CA slates investigated in this study were provided by Tecneco Srl, a company specialized in asbestos removal and disposal. About 40 kg of CA slates, all coming from the same locality, were treated at 1100 °C in air in three separate runs in a Nabartherm static furnace model HT160/17 of 150-liter capability (500x550x550 mm). Details of the inertization process are reported in the supplementary Table S1. Representative parts of the samples were analysed before and after treatment with a multi-methodological approach, as detailed below.

2.2. X-Ray Powder Diffraction (XRPD)

XRPD analyses were performed on representative, as-received bulk samples and on treated samples. Samples were grinded in agate mortar and back loaded into an Al sample holder. The XRPD study was conducted using a Bragg–Brentano PANalytical X'Pert-Pro PW3060 diffractometer with θ–θ geometry and CuKα radiation, in the 5–80° 2θ range with step size of 0.02°, at room temperature and operating conditions of 40 mA and 40 kV. Qualitative phase analysis was carried out with the PANalytical X'Pert High Score software, using the ICSD PDF2-2004 database. For quantitative phase analysis (QPA), 20 wt% of α-alumina (NIST SRM 676a) was added as internal standard. QPA was performed with the Rietveld method [23] using the GSAS package [24] and the graphical interface EXPGUI [25]. The weight fraction of each crystalline phase (W_α') in the studied samples was quantified according to the following equation:

$$W_\alpha' = W_\alpha \frac{W_c'}{W_c}\left(\frac{1}{1-W_c'}\right)$$

where W_α and W_c are the refined weight fractions of phase α and of the internal corundum standard, respectively, and W_c' is the actual added weight of the internal standard (10 wt%). The actual weight fraction of the amorphous material (W_g') is then calculated as $W_g' = 1-\Sigma_i W_{\alpha i}'$. According to Gualtieri [26], the relative error in glass content quantification is around 10% for fractions of the amorphous phase greater than 10 wt% and increases with decreasing weight fraction of the glass.

2.3. Energy Dispersive X-Ray Fluorescence Spectrometry (EDXRF)

Bulk chemical analyses of the as-received and inert samples were obtained with a PANanalytical Epsilon 3X energy dispersive X-ray fluorescence (EDXRF) instrument. Sample briquettes were prepared by mixing 15 g of powdered material, 5 g of boric acid and few drops of polyvinyl alcohol. Briquettes were pressed at a pressure of 15.000 kg/cm^2 for a minute and then left for 2-3 hours at 60 °C to eliminate any water adsorbed during the preparation. The Omnian-standardless method was used for quantitative analyses. Aliquots of the powder were used for volatile components (H_2O plus CO_2) determination through weight loss on ignition (LOI) and Fe^{3+}/Fe^{2+} ratio determination through $KMnO_4$ redox titration.

2.4. Scanning Electron Microscopy (SEM)

SEM investigations were performed with a Tescan VEGA TS 5136XM equipped with an EDAX Genesis 4000 energy dispersive system (EDS) and a Zeiss Gemini 500 equipped with a Bruker XFlash 6I30 EDS. The observations were focused on pristine fibers and pseudomorphs of the original fibres after thermal treatment and recrystallization. Fragments of samples were positioned on aluminium stubs carrying bi-adhesive carbon pads and either carbon or gold coated. The latter was necessary for high resolution observations with the Zeiss instrument, which requires higher vacuum and therefore higher sample conductivity.

2.5. Transmission Electron Microscopy (TEM)

TEM investigations were performed with a JEOL JEM 2100P instrument, operating at 200 kV and equipped with an Oxford EDS spectrometer and a Gatan Rio CMOS camera for image acquisition. The observations were focused on pseudomorphs of the original fibres. Since still recognizable after the treatment under a stereomicroscope, few fibres were picked up with a tweezer, gently powdered in isopropyl alcohol and ultrasonicated for 3 minutes. 5 μL of the suspension was then deposited on 300 mesh Cu grids supporting a C membrane.

2.6. Dynamic Laser Scattering (DLS)

After thermal treatment, although fragile, inert slates are self-sustaining. Therefore, milling is probably required before any reuse. The treated samples were first grinded with a hydraulic press down to a gran size lower than 2 mm. Then, different parts of the coarse powder were reduced with a ball mill for milling times of 5, 10, 15 and 25 minutes, the latter alternating the sense of rotation after 15 minutes. The grain size distributions for all these samples were obtained with a Malvern Mastersize APA 2000 DLS apparatus, using a 445 nm wavelength (blue).

2.7. Leaching Experiments

For leaching experiments, 2 g of the powdered inert material was added in previously cleaned plastic cuvettes containing 20 mL mQ water (18.2 $M\Omega \cdot cm^{-1}$). The experiments were performed at room temperature (~25 °C) on a table shaker (stirring at 150 rpm), in order to ensure an efficient mixing of the suspension. The stirring durations were 1 hour, 1 day and 14 days, respectively. The employed grain sizes varied from 71 μm to 0.45 μm (15 min milling, see ahead). At the end of the leaching experiments, the suspensions were centrifuged for 10 min at 3500 rpm and filtrated immediately with a 0.20 μm acetate filter. Concentrations of alkaline (Li^+, Na^+, K^+), Ca^{2+} and Mg^{2+} cations and anions (F^-, Cl^-, Br^-, NO_3^{2-}, SO_4^{2-}, PO_4^{3-}, NO_2^{2-}) of the leachates were determined by ion exchange chromatography (IEC) using a Metrohm 883 Basic IC Plus. For anions, a dilute solution 3.2 mM of Na_2CO_3 and 1.0 mM of $NaHCO_3$ was used. For cations, a dilute solution 100 mM di H_2SO_4 was used. Si and transition metals (Fe, Zn, Cu, Mn, Al, Ba, Cr, Ti, V,

Sn) were measured with graphite furnace atomic absorption spectroscopy (GFAAS) using an AAnalyst 600 PerkinElmer instrument. Pb and Ni were measured by inductively coupled plasma optical emission spectrometry (ICP-OES) using an Optima 7000 DV PerkinElmer instrument. Calibration solutions were prepared with a 2% and a 0.2% HNO_3 solutions for ICP-OES and GFAAS, respectively.

3. Results

3.1. Untreated samples

Two apparently different types of CA slates were investigated, flat tiles and classical undulated tiles, coming both from the same dismantled installation. The samples were investigated by XRPD, EDXRF and SEM-EDS. Within the experimental limit of the mentioned techniques, there is no relevant difference in terms of mineralogy, texture and composition between the two types of ACM. The bulk chemical composition of the untreated samples is reported in supplementary Table S2. CaO, SiO_2, MgO, Fe_2O_3, Al_2O_3 and SO_3 are the major components. All the other components occur at concentration lower than 1 wt%.

The main detected phases with XRPD are calcite, quartz, chrysotile and crocidolite (traces). In addition, SEM-EDS investigations revealed the presence of minor zircon and barite. Moreover, among the fibrous minerals, chrysotile is by far the most abundant, whereas crocidolite is rare, as well as tremolite-actinolite, the latter not detected by XRPD. In Figure 1 we report the texture of the original CA slate, along with some representative EDS spectra of the fibrous minerals. In general, chrysotile fibers are comparatively wavier than amphibole fibers; however, in the present case, distinction between amphibole and chrysotile was possible only based on chemical composition (see Fig. 1).

3.2. Treated samples

3.2.1. EDXRF and XRPD bulk analyses

The bulk chemical composition of the treated sample (Table 1, left) is consistent with that of the untreated sample once realized that volatiles escaped during high temperature thermal inertization. Some of the minor and trace elements detected in the untreated samples, notably P, Cl, Cr, Ni, Zn, Sr and Ba could not be detected at significant level in the treated samples. A possible explanation is that the volatilization of light components such as CO_2 and H_2O, occurring during thermal inertization, produced significant changes in the matrix (densification). This in turn affected the matrix correction algorithm that lowered the sensibility to trace elements. The LOI is very low (0.32 wt%), suggesting that the sample did not reabsorb humidity after the short lapse of time between the treatment and the analysis (two weeks). XRPD analyses revealed as glass major constituents akermanite, bredigite, merwinite and larnite (Table 4, right). The Ca-Mg silicates are common cement phases and result from the reaction at high temperature of the original calcite

ligand, quartz filler and chrysotile and crocidolite asbestos and represents 3/5 of the bulk. Their chemical compositions accounts for the major bulk chemical components, apart some Al_2O_3, Fe_2O_3, and minor components (MnO, TiO_2), which are not considered in the ideal formula of the reported phases, but that can be present as solid solutions in the actual crystalline phases, as well as in the silicate glass. Glass may also account for the alkaline components Na_2O and K_2O, known to be fluidophile [27]. The provenance of the SO_3 is doubtful. Some studies [19] report SO_3 to be present in the high temperature phase silicocarnotite [$Ca_5(SiO_4)_2SO_4$)], but it could not be safely identified in our samples. A possible explanation is that SO_4^{2-} anions could substitute for SiO_4^{4-} in the framework of the silicate phases reported above.

3.2.2. SEM-EDS and TEM-EDS on fiber pseudomorphs

SEM-EDS observations were focused on pseudomorphs of the original asbestos fibers detected on fresh fractures of the inertized slates. Some representative images are reported in Figure 2A to D. The fiber pseudomorphs can be easily recognized at low magnification, whereas at high magnification the pervasive recrystallization in micrometric grains is evident. This microstructure suggests that the original cleavage of the fibers parallel to the fiber length is superseded by a parting along grain boundaries in treated samples, excluding the formation of hazardous fibrils. EDS analyses of several grains gave systematically Ca, Si, Al, Mg and Fe as major cations, although with different reciprocal abundances from grain to grain. Minor Na, P and S can be also detected; the latter may be locally abundant (Fig. 2F). Given the very small grain size in comparison with the electron beam penetration (~5μm at 20 keV), it is very probable that the spectra could result from mixed compositions of different grains, rather than chemically different single grains. TEM/EDS observations were focused on fibre pseudomorphs, after grinding and deposition on carbon membranes (Fig. 3). It is worth noting that the fibres are completely recrystallized in microscopic and sub-microscopic equidimensional grains and no trace of fibrils, the harmful small acicular crystals in which the asbestos fibres split under grinding, can be recognized. Grains may have either round or sharp edges and conchoidal fracture is often observed. Chemical spot analyses were collected on several grains, which in most cases gave a spectrum consistent with forsterite, confirmed also by the selected area electron diffraction SAED (Fig. 3D and E). Some grains show Ca, Al and Fe peaks and lower Mg (Fig. 3F), but could not be reconciled with any certain phase. Finally, other grains show Si as the dominant cation, along with minor amount of Al and Mg and significant amount of alkali (Na and K) and Fe (Fig. 3G). The latter may represent glass, since it is notorious that partial melting in many Ca-Mg-Al-Si-Fe-alkali systems gives a melt enriched in Si, Fe and alkali and depleted in refractory Ca, Al and Mg [28].

3.2.3. DLS results

Disregarding the milling time, all powdered samples show a three-modal grain size distribution, with maxima at grain size comprised between ~25-40 μm, ~3.5-5.6 μm and ~0.7-0.9 μm (Table 2). It should be noted, however, that the relative abundance of gran sizes changes with the milling time. The larger grain size (35-40 μm) is the most abundant for the lowest milling time (5 min) and the less abundant for milling time of 25 min (Fig. 4). The smallest grain size increases significantly for milling times exceeding 5 min, it is the less abundant for milling time lower than 15 min, but exceeds the largest grain size for milling time of 25 min. The intermediate grain size is peaked at ~5-5.6 μm for milling time of 5 min, and at 3.5-4 μm for milling times exceeding 5 min; it becomes the most abundant for milling times exceeding 5 min.

As regard the relative abundances expressed as airborne particulate matter classes, PM10, PM2.5 and PM1, that is particles with aerodynamic diameter lower than 10 μm, 2.5 μm, and 1 μm, respectively, all increases with increasing milling time, but their volume fraction steeply increases for milling times exceeding 5 min.

3.2.4. Leaching tests

Leaching test results are reported in Table 3 and graphically for the relevant elements in Figure 5. The pH pf the solution is much higher in the leachates than in the eluent (7) only after 1 hr of leaching (11.68), then increase slightly with leaching time (12.05 after 14 days). This is paralleled by the concentration of Ca (360-377 ppm), K (296-302 ppm) and Na (125-178 ppm), which are the major alkaline/earth-alkaline cations detected in the leachates at any time and that remain almost constant within the two-weeks observation period. Mg (0.50-1.40 ppm), although more abundant than Na and K in the bulk, is present only at ppm level in the leachate, it increases with time after one hour and it is not detected in the two-weeks sample, probably because it precipitates for the longest leaching time, and therefore not detected in solution. Among the anions, SO_4^{2-} (1237-1534 ppm) is by far the most abundant, followed by Cl^- (7.34-7.77 ppm), NO_3^{2-} (0.58-2.14 ppm), and F^- (0-1.95 ppm) anions, in the order. SO_4^{2-} and Cl^- remain barely constant along the observation period, whereas NO_3^{2-} increases and F^- decreases. Among the metals, Si (0.11-20.10 ppm) is by far the most abundant, consistently with the bulk composition, but decreases drastically after two-weeks leaching. Unpredictable relatively high level of Cr (6.12-7.23 ppm) is detected, which remains almost constant during the observation period. Significant levels of Al (0.99-1.31 ppm), which increases with time, and Ba (0.09-0.48 ppm), which decreases, are also detected. We detected also minor amounts of V (0.03-0.04 ppm) and Cu (0.002-0.007 ppm), whereas Fe, although abundant component of the bulk material, is below the detection limit in the leachate. A possible explanation of this observation is provided by the oxidizing atmosphere of ACW thermal inertization (in air), that favours the occurrence of Fe as Fe^{3+}, which is relatively insoluble. Alternatively, Fe underwent very fast precipitation (within 1 hr) after leaching.

4. Discussion

4.1. Process conditions vs. inert composition

Thermal inertization of CA slates in air at 1100 °C is an effective method for the irreversible crystal-chemical transformation of asbestos fibres into harmless phases. The overall treated material is mostly composed of Ca-Mg silicates and glass, therefore compositionally similar to a Mg- and Fe-rich clinker.

In their study on high temperature transformation of CA slates, Viani et al. [21] demonstrated that ACW with different starting Si, Ca, and Mg proportions, lead to the growth of cement phases in different quantitative proportions. The chemical and mineralogical compositions of the thermally transformed product affect its possible reuse as secondary raw material. However, the maximum temperature of the heating process along with kinetic factors affect the finale phase composition [19, 21]. Firing temperature up to 1200°C yields to akermanite, merwinite, larnite, ferrite and an amorphous phase [19]. Firing temperature up to 1250°C, with different heating steps, yields to three main mineral assemblages with different proportion of Ca and Ca/Mg silicate phases, depending upon the initial CaO/SiO_2 (C/S) ratio [21]. Larnite-rich assemblage occurs for C/S ratio close to 1.5; lower ratios give rise to bredigite and akermanite-rich samples, with the latter prevailing at the lowest C/S ratios. After inertization at 1150°C, the samples studied by Marian et al. [18] characterized by a C/S ratio between 1.71 and 2.18 consistently show a larnite-rich composition, coexisting with a very high glass content.

In the present paper, after heating at 1100°C, the resulting material consists of akermanite-bredigite-merwinite in similar proportion (19.33%, 19.25%, 17.84%, respectively) with an initial C/S ratio of 1.5. The predominance of Mg-Ca silicates is probably due to the lower firing temperature and different process conditions in terms of heating rate, annealing temperature, annealing time, kind of atmosphere with respect to the previously quoted papers. In summary, although in all these cases the toxic asbestos fibres are deactivated, the resulting product may show different proportions of cement phases, glass and oxides, demonstrating the importance, other than the ACW starting chemical composition, of the process conditions on the final mineralogical composition, which in turn affects the reuse applications.

4.2. Nano-fraction concern

According to the Italian Ministry Decree 12/2/97, the product of ACW crystal-chemical transformation can be safely recycled if the following requirements are satisfied: (i) it must be entirely asbestos-free; (ii) it should not contain more than 0.1 wt% of carcinogenic substances such as cristobalite; (iii) it may contain fibrous phases (length to diameter ratio > 3 μm) other than asbestos if their geometrical diameter is >3 μm; (iv) the content of fibrous phases with a geometrical

diameter <3 μm should be <20% of the total fiber content; (v) it should not contain fibers that, despite their diameter, exhibit a cleavage parallel to the fiber axis. All these requirements are satisfied by the studied treated material. However, DLS analysis of the powdered SRM reveals that a significant number of grains falls in the PM1 range, and TEM images show that a significant amount of them are nanoparticles, i.e. particles with all the three dimensions smaller than 100 nm. Because of the importance of nanoparticles in many modern technological applications and processes, their production has increased dramatically in recent years, along with the dispersion in the environment and the concern about their effect on life beings and human health – for a recent review see ref. [29]. Inhalation is the most common routes of human exposure: nanoparticles can penetrate the alveolar-capillary membrane, reach the bloodstream and then distribute to peripheral organs. The liver is the primary organ of detoxification biological filter and is one of the tissues that is most exposed to nanoparticles). The question about the safety of these nanomaterials and their impact on human health is therefore a legitimate concern [30-36].

As far as we know, only a few studies exist on cytotoxicity of inert SRM material, none especially dedicated to nanoparticles. Giantomassi et al. [37], in a comparative study on human alveolar epithelial cells, have reported that the product of transformation of cement-asbestos at 1200 °C (KRY·AS) has considerably lower cytotoxic than the original asbestos material. Gualtieri et al. [38], in an in vitro biodurability study, reported that KRY-AS has lower biodurability than chrysotile asbestos. These studies prove the low potential toxicity of the thermal transformed ACW but leave an open question about the cytotoxicity and eco-compatibility of the nanosized fraction.

4.3. Possible routes to control the grain size distribution

On the one hand, the microstructure evidenced by SEM and TEM is reassuring, since the pseudomorphic fibers are still recognizable after thermal treatment but do not show the cleavage parallel to the fiber axis able to generate dangerous fibrils. On the other hand, it seems that the pervasive recrystallization occurring at a very fine scale of fibers and cement can govern the grain size distribution of the final SRM. Indeed, DLS experiments have demonstrated that even significantly varying the milling parameters, the grain size distribution is only partially affected. The grain size is an important parameter in many applications and, as discussed above, it may pose health-related issues, hence the need for effective methods for controlling the grain size of the transformed material.

Once again, the process conditions turn out decisive. It is well known from petrological studies and crystal growth experiments that heating rate, annealing temperature and cooling rate are effective parameters in determining grains size of rocks and materials [39-40]. For instance, a fine-grained limestone (micrite) become a marble with saccharoidal (mm-sized) structure after thermal annealing at high temperature [41]. A basic magma forms a fine grain size rock (diabase) if crystallizes under fast cooling rate at shallow depth, whereas the same magma forms a coarse grain size

rock (gabbro) if crystallizes deeply in the crust. Similar concepts are adopted at laboratory scale to condition the grain size of the synthetic rocks and materials. It is therefore predictable that by fine tuning the process conditions, the grain size distribution of the treated ACW can be controlled.

A further strategy aiming at controlling the grain size distribution of the treated material is represented by the microwave controlled comminution before ball milling. Microwave has been demonstrated effective in reducing the comminution time in mine processing operations [42-48]. Rapid heating of ore minerals and rocks in a microwave transparent matrix generates thermal stress of sufficient magnitude to create microcracks along mineral boundaries. The efficiency of the breakage depends on operating parameters such as microwave power, exposure time, distance from the antenna. In the present contest, the goal may be either avoiding the finest grain size that may pose health related problems or, conversely, the obtainment of a larger aliquot of the finest grain size for specific applications. In the first case, the application of microwave irradiation may be coupled with a reduction of the ball milling time. Indeed, we have seen above that increasing the milling time the aliquot of the finest particles increases. The microwave induced microcracking has the potential to improve grinding efficiency without leaving coarse particles in the mixture, with the net results of moving the grain size median upwards. The second case may be applied whenever the finest grain size is not fine, or not abundant enough. This may be the case in applications with composite materials. These are made by mixing materials of different nature, such as organic polymers and inorganic particles, with the aim of obtaining products that retain the best of both. The main obstacle in pursuing such objective is that different components tend to be chemo-physically incompatible and separate at the microscopic level, producing filler aggregates, defects and ultimately the loss of the desired properties. The nanometer scale at which the inert material can be reduced with the aid of microwave assisted comminution lets us envisage a profitable strategy to make compatible the organic matrix and the inorganic filler. That relies on the possibility to form chemical bonds between the inorganic nanoparticles surface and the polymer chains. This can be achieved by the “grafting to” method, that is the attachment of previously prepared polymer chains to the nanoparticle surface via a reactive chain end [49], or by the “grafting from” one, that is growing directly the polymer on reactive sites present on the nanoparticle surface [50].

4.4. Implication of SO_4 and Cr in the leachate

The leaching tests performed on the powdered SRM (10 min milling time) should be considered as an extreme case of interaction with the aquatic environment, since in normal conditions the inert powder should be used as a diluted component in solid objects, either with ceramic or polymeric structure, which may or may not entail a liquid medium during the manufacturing process. On the other hand, during the shelf life, the inert powder should be maintained in sealed bags, as for other inorganic raw materials, therefore sheltered from accidental elemental release on aqueous

media. A liquid medium is certainly needed during the manufacturing process of ceramic artifacts. In this case, a high level of SO_4^{2-} can reduce the zeta potential of the clay particles increasing the viscosity of the paste, then necessitating a higher deflocculant addition to make the paste workable, raising the production costs [51].

A hydrous phase is involved also in the execution of concrete works. Ideal Portland cement usually contains ~1.7 wt% of SO_3 component, usually in the form of gypsum ($CaSO_4 \cdot 2H_2O$), which is ~5 wt% [52]. Gypsum is usually added to the clinker to act as a setting time regulator. Portland cement is the main binder in concrete characterized by high mechanical strength, high heat of hydration, but poor resistance to acid attack. Sulphate ions can react with calcium aluminate components of cement forming further gypsum during curing. The newly formed gypsum crystals occupy empty spaces of concrete, and as they grow, tend to damage the paste by cracking. A way to control this problem is to lower the calcium aluminate component by pozzolanic admixture, which moves to overall composition towards a SiO_2 richer one [53]. The secondary raw material studied here has a composition higher in SiO_2 than normal clinker, therefore we can tentatively assume that the adverse effects of SO_4^{2-} addition could be balanced by the increase of SiO_2 component. Alternatively, part of the gypsum in the Portland cement formulation can be substituted by limestone [54-55].

The comparison of the results of the leaching tests with the contamination threshold limits for groundwater reported in the Italian Law D. Lgs. 152/06 [56], reveals values slightly above the limit only for Cr (threshold limit 5 ppm; measured values 6.12-7.23 ppm) in the case that Cr could be hexavalent. We did not measure the oxidation state of Cr, but since the inertization processes occurred in air, it is very probable that Cr could be totally oxidized.

Contamination of groundwater can occur in the remote case that the SRM is stored in an open, permeable environment and infiltrated by rainwater, i.e., if it is used as soil. The same D. Lgs. 152/06 reports a concentration threshold limit for Cr^{6+} of 2 ppm for terrains (soil and subsoil) intended for civilian uses (public, private and residential green), and 15 ppm in case of terrains intended for commercial and industrial uses. From the above considerations, we conclude that the SRM cannot be used as soil conditioning.

In the even more remote case that SRM seepage water could flow into drinking water supplies, the concentration of F^- (up to 1.95 ppm) and SO_4^{2-} (1237-1492 ppm) should be carefully considered because, according to the European drinking water directive 98/83/EC [57], they exceed the drinkable limits for public waters (1.5 ppm and 250 ppm, respectively). These are of considerable concern since F^- increases the risks of dental and skeletal fluorosis [58], and SO_4^{2-} adds a salty taste to the water and causes consumers to suffer of gastrointestinal irritation and diarrhea [59].

5. Conclusions

Thermal inertization of cement-asbestos slates at 1100°C in air is effective in the crystal-chemical transformation of asbestos fibers into harmless particles attributable to cement phases. However, the mineralogical composition and the grain size distribution of the inert SRM may vary as a function of the inertization parameters (heating rate, annealing temperature, cooling rate, etc.). This in turn may affect the recycling applications. As regard the particle size distribution, a significant fraction of nanoparticles is produced, which may pose environment and human health concern. Tests on thermal treatment conditions aiming to establish a correlation with the particle size distribution are envisaged. Moreover, microwave-assisted comminution combined with ball milling is proposed as a strategy to better constrain the grain size. Leaching test results on the powdered SRM evidenced some critical release of SO_4^{2-}, F^- and Cr^{6+}. Sulphates may have adverse effects on potential applications of the SRM in the ceramic and cement industries. Hexavalent Cr is highly toxic, and caution must be paid to impede the arrival of any SRM leachate to drinking water supplies. Fluorine and sulphate, although they are not toxic as Cr^{6+}, may cause to the consumer dental and skeletal fluorosis the former, salty taste and gastrointestinal problems the latter. Both should not arrive through seepage waters to drinking water supplies. This is a remote possibility since the most promising industrial applications of the SRM (ceramic and cement industry) dilute such contaminants – the SRM is admixed in few percent – and prevent their leaching – the SRM is tightly embedded in a matrix. Eventually, the SRM is not recommended the reuse as soil conditioning.

Acknowledgements

This work is an outcome of the project DEAR: Deativazione Efficiente dell'Amianto e Riutilizzo, funded by the Italian Ministry of the Ecologic Transition.

Conflicts of interest/Competing interests: The authors declare that they have no conflicts of interest or competing interests.

Authors' contributions: All authors contributed to the study conception and design. Material preparation, data collection and analysis were performed by Fabrizio Vergani, Lucia Galimberti and Giancarlo Capitani. The first draft of the manuscript was written by Fabrizio Vergani e Giancarlo Capitani and all authors commented on previous versions of the manuscript. All authors read and approved the final manuscript.

References

[1] Bentur A, Mindess S (2007) Fibre reinforced cementitious composites, CRC Press, London.

[2] Legge 27 marzo 1992, n. 257, Norme relative alla cessazione dell'impiego dell'amianto, GU Serie Generale n.87 del 13-04-1992 - Suppl. Ordinario n. 64. https://www.gazzettaufficiale.it/eli/id/1992/04/13/092G0295/sg

[3] Decreto 29 luglio 2004, n. 248, Regolamento relativo alla determinazione e disciplina delle attività di recupero dei prodotti e beni di amianto e contenenti amianto, GU Serie Generale n.234 del 05-10-2004. https://www.gazzettaufficiale.it/eli/id/2004/10/05/004G0280/sg

[4] ISPRA, 2020. Rapporto Rifiuti Speciali. https://www.isprambiente.gov.it/files2020/pubblicazioni/rapporti/rapportorifiutispeciali_ed-2020_n-321_versioneintegrale_agg02_10_2020.pdf

[5] European Parliament resolution of 14 March 2013 on asbestos related occupational health threats and prospects for abolishing all existing asbestos (2012/2065(INI)). https://www.europarl.europa.eu/doceo/document/TA-7-2013-0093_EN.html

[6] Spasiano D, Pirozzi F (2017) Treatments of asbestos containing wastes. J Environ Manage 204:82–91. https://doi.org/10.1016/j.jenvman.2017.08.038

[7] Inaba T, Nagano M, Endo M (1999) Investigation of plasma treatment for hazardous wastes such as fly ash and asbestos. Electr Eng Japan 126:73–82. https://doi.org/10.1002/(SICI)1520-6416(199902)126:3<73::AID-EEJ8>3.0.CO;2-J

[8] Inaba T, Iwao T (2000) Treatment of waste by dc arc discharge plasmas. IEEE Trans Dielectr Electr Insul 7:684–692. https://doi.org/10.1109/94.879362

[9] Colombo P, Brusatin G, Bernardo E, Scarinci G (2003) Inertization and reuse of waste materials by vitrification and fabrication of glass-based products. Curr Opin Solid State Mater Sci 7:225–239. https://doi.org/10.1016/j.cossms.2003.08.002

[10] Tu X, Yu L, Yan J, Cen K, Chéron BG (2010) Plasma Vitrification of Air Pollution Control Residues From Municipal Solid-Waste Incineration. IEEE Trans Plasma Sci 38:3319–3325. https://doi.org/10.1109/TPS.2010.2056939

[11] Finucane KG, Thompson LE, Abuku T, Nakauchi H (2008) Treatment of Asbestos Wastes Using the GeoMelt® Vitrification Process. WM2008 Conference Phoenix AZ, 1–10. http://archive.wmsym.org/2008/pdfs/8261.pdf

[12] Dellisanti F, Rossi PL, Valdrè G (2009) Remediation of asbestos containing materials by Joule heating vitrification performed in a pre-pilot apparatus. Int J Miner Process 91:61–67. https://doi.org/10.1016/j.minpro.2008.12.001

[13] Bernardo E, Esposito L, Rambaldi E, Tucci A (2011) Sintered glass ceramic articles from plasma vitrified asbestos containing waste. Adv Appl Ceram 110:346–352. https://doi.org/10.1179/1743676111Y.0000000020

[14] Abruzzese C, Marabini AM, Paglietti F, Plescia P (1998) CORDIAM process: A new treatment for asbestos wastes. In: Mishra B (ed), EPD Congress, San Antonio TX USA, TMS Springer, Boston, pp. 563–577.

[15] Belardi G, Maccari D, Marabini AM, Plescia P (1998) Process for producing ceramic type materials by processing waste containing asbestos and clay. Patent No WO199822410A1.

[16] Gualtieri AF, Zanatto I (2009) Industrial Process for the Direct Temperature Induced Recrystallization of Asbestos and/or Mineral Fibers Containing Waste Products Using a Tunnel Kiln and Recycling, European Patent No. EP07425495.

[17] Gualtieri AF, Giacobbe C, Sardisco L, Saraceno M, Lassinantti Gualtieri M, Lusvardi G, Cavenati C, Zanatto I (2011) Recycling of the product of thermal inertization of cement-asbestos for various industrial applications. Waste Manag 31:91–100. https://doi.org/10.1016/j.wasman.2010.07.006

[18] Marian NM, Giorgetti G, Magrini C, Capitani GC, Galimberti L, Cavallo A, Salvini R, Vanneschi C, Viti C (2021) From hazardous asbestos containing wastes (ACW) to new secondary raw material through a new sustainable inertization process: A multimethodological mineralogical study. J Hazard Mater 413:125419.

[19] Gualtieri AF, Cavenati C, Zanatto I, Meloni M, Elmi G, Lassinantti Gualtieri M (2008) The transformation sequence of cement-asbestos slates up to 1200°C and safe recycling of the reaction product in stoneware tile mixtures. J Hazard Mater 152:563–570. https://doi.org/10.1016/j.jhazmat.2007.07.037

https://doi.org/10.1016/j.jhazmat.2021.125419

[20] Gualtieri AF, Boccaletti M (2011) Recycling of the product of thermal inertization of cement-asbestos for the production of concrete. Constr Build Mater 25:3561–3569. https://doi.org/10.1016/j.conbuildmat.2011.03.049

[21] Viani A, Gualtieri AF, Pollastri S, Rinaudo C, Croce A, Urso G (2013) Crystal chemistry of the high temperature product of transformation of cement-asbestos. J Hazard Mater 248–249:69–80.

https://doi.org/10.1016/j.jhazmat.2012.12.030

[22] Ligabue ML, Gualtieri AF, Lassinantti Gualtieri M, Malferrari D, Lusvardi G (2020) Recycling of thermally treated cement-asbestos for the production of porcelain stoneware slabs. J Clean Prod 247:119084.

https://doi.org/10.1016/j.jclepro.2019.119084

[23] Rietveld HM (1969) A profile refinement method for nuclear and magnetic structures. J Appl Crystallogr 2:65–71.

https://doi.org/10.1107/S0021889869006558

[24] Larson AC, Von Dreele RB (1994) Generalized Structure Analysis System (GSAS). Los Alamos National Laboratory Report LAUR 86−748.

[25] Toby BH (2001) EXPGUI, a graphical user interface for GSAS. J Appl Crystallogr 34 :210–213.

https://doi.org/10.1107/S0021889801002242

[26] Gualtieri AF (2000) Accuracy of XRD QPA using the combined Rietveld-RIR method. J Appl Crystallogr 33:267–278. https://doi.org/10.1107/S002188989901643X

[27] Shelby JE (2020) Introduction to glass science and technology, Royal Society of Chemistry, London.

[28] Frost BR, Frost CD (2014) Essentials of Igneous and Metamorphic Petrology, ed. Cambridge University Press, New York. https://doi.org/10.1017/9781108685047

[29] Martínez G, Merinero M, Pérez-Aranda M, Pérez-Soriano EM, Ortiz T, Begines B, Alcudia A (2021) Environmental impact of nanoparticles' application as an emerging technology: A review. Materials (Basel). 14:1–26. https://doi.org/10.3390/ma14010166

[30] Buzea C, Pacheco II, Robbie, K (2007) Nanomaterials and nanoparticles: sources and toxicity. Biointerphases 2:MR17. https://doi.org/10.1116/1.2815690

[31] De Jong WH, Borm PJA (2008) Drug delivery and nanoparticles: applications and hazards. Int J Nanomed 3:133. https://doi.org/10.2147/ijn.s596

[32] Aydın A, Sipahi H, Charehsaz M (2012) Nanoparticles toxicity and their routes of exposures. In: Sezer AD (ed) Recent Advances Novel Drug Carrier Systems, Intech Open. https://doi.org/10.5772/51230

[33] Brown JS, Gordon T, Price O, Asgharian B (2013) Thoracic and respirable particle definitions for human health risk assessment. Part Fibre Toxicol. 10:12. https://doi.org/10.1186/1743-8977-10-12

[34] Zoroddu MA, Medici S, Ledda A, Nurchi VM, Lachowicz JI, Peana M (2014) Toxicity of nanoparticles. Curr Med Chem 21:3837–3853. https://doi.org/10.2174/0929867321666140601162314

[35] Maher BA, Ahmed IAM, Karloukovski V, MacLaren DA, Foulds PG, Allsop D, Mann DMA, Torres-Jardón R, Calderon-Garciduenas L (2016) Magnetite pollution nanoparticles in the human brain. Proc Natl Acad Sci USA 113:10797–10801. https://doi.org/10.1073/pnas.1605941113

[36] Bencsik A, Lestaevel P, Guseva Canu I (2018) Nano- and neurotoxicology: An emerging discipline. Prog Neurobiol 160:45–63. https://doi.org/10.1016/j.pneurobio.2017.10.003

[37] Giantomassi F, Gualtieri AF, Santarelli L, Tomasetti M, Lusvardi G, Lucarini G, Governa M, Pugnaloni A (2010) Biological effects and comparative cytotoxicity of thermal transformed asbestos-containing materials in a human alveolar epithelial cell line. Toxicol Vitr 24:1521–1531. https://doi.org/10.1016/j.tiv.2010.07.009

[38] Gualtieri AF, Veratti L, Tucci A, Esposito L (2012) Recycling of the product of thermal inertization of cement-asbestos in geopolymers. Constr Build Mater 31:47–51. https://doi.org/10.1016/j.conbuildmat.2011.12.087

[39] Hammer JE (2008) Experimental Studies of the Kinetics and Energetics of Magma Crystallization. Rev Mineral Geochem 69:9–59. https://doi.org/10.2138/rmg.2008.69.2

[40] Johannes W, Holtz F (2012) Petrogenesis and experimental petrology of granitic rocks, Springer Science & Business Media, Berlin. https://www.springer.com/it/book/9783642646713

[41] Kahl W-A (2015) Essentials of Igneous and Metamorphic Petrology. Cambridge University Press, U.K. https://doi.org/10.2138/am-2015-657

[42] Kingman SW, Corfield GM, Rowson NA (1970) Effects of microwave radiation upon the mineralogy and magnetic processing of a massive Norwegian ilmenite ore. Magn Electr 9:131-148. https://downloads.hindawi.com/archive/1999/057075.pdf

[43] Kingman SW, Jackson K, Cumbane A, Bradshaw SM, Rowson NA, Greenwood R (2004) Recent developments in microwave-assisted comminution. Int J Miner Process 74:71–83. https://doi.org/10.1016/j.minpro.2003.09.006

[44] Haque KE (1999) Microwave energy for mineral treatment processes - A brief review. Int J Miner Process 57:1–24. https://doi.org/10.1016/s0301-7516(99)00009-5

[45] Vorster W, Rowson NA, Kingman SW (2001) The effect of microwave radiation upon the processing of Neves Corvo copper ore. Int J Miner Process 63:29–44. https://doi.org/10.1016/S0301-7516(00)00069-7

[46] Lovás M, Znamenáčková I, Zubrik A, Kováčová M, Dolinská S (2011) The application of microwave energy in mineral processing–a review. Acta Montan Slovaca 16:137-148. https://actamont.tuke.sk/pdf/2011/n2/4lovas.pdf

[47] Hassani F, Nekoovaght PM, Gharib N (2016) The influence of microwave irradiation on rocks for microwave-assisted underground excavation. J Rock Mech Geotech Eng 8:1–15. https://doi.org/10.1016/j.jrmge.2015.10.004

[48] Teimoori K, Cooper R (2021) Multiphysics study of microwave irradiation effects on rock breakage system. Int J Rock Mech Min Sci 140:104586. https://doi.org/10.1016/j.ijrmms.2020.104586

[49] Selli D, Tawfilas M, Mauri M, Simonutti R, Di Valentin C (2019) Optimizing PEGylation of TiO_2 Nanocrystals through a Combined Experimental and Computational Study. Chem Mater 31:7531–7546. https://doi.org/10.1021/acs.chemmater.9b02329

[50] Crippa M, Bianchi A, Cristofori D, D'Arienzo M, Merletti F, Morazzoni F, Scotti R, Simonutti R (2013) High dielectric constant rutile-polystyrene composite with enhanced percolative threshold. J Mater Chem C 1:484–492. https://doi.org/10.1039/c2tc00042c

[51] Jantzen CM, Smith ME, Peeler DK (2004) Dependency of sulfate solubility on melt composition and melt polymerization. Ceram Trans 168:141–152. https://scholar.google.com/scholar?hl=it&as_sdt=0%2C5&q=Dependency+of+sulfate+solubility+on+melt+composition+and+melt+polymerization&btnG=

[52] Dunuweera S, Rajapakse R (2018) A Brief Overview on Chemical and Physical Aspects of Archaeological Dating Techniques and Their Applications in Dating Construction Materials and Buildings. Asian J Phys Chem Sci 6:1–13. https://doi.org/10.9734/ajopacs/2018/40349

[53] Lawrence CD (1990) Sulphate attack on concrete. Mag Concr Res 42:249–264. https://doi.org/10.1680/macr.1990.42.153.249

[54] Bensted J (1980) Some hydration investigations involving portland cement-effect of calcium carbonate substitution of gypsum. World Cem Technol 11:395-406.

[55] Bensted J (1983) Further hydration investigations involving Portland cement and the substitution of limestone for gypsum. World Cem Technol 14:383–392.

[56] Decreto Legislativo del 3 aprile 2006, n. 152, Norme in materia ambientale, GU Serie Generale n.88 del 14-04-2006 - Suppl. Ordinario n. 96. https://www.gazzettaufficiale.it/dettaglio/codici/materiaAmbientale

[57] European Council Directive 98/83/EC of 3 November 1998 on the quality of water intended for human consumption. https://ec.europa.eu/environment/water/water-drink/legislation_en.html

[58] Stewart C, Johnston DM, Leonard GS, Horwell CJ, Thordarson T, Cronin SJ (2006) Contamination of water supplies by volcanic ashfall: A literature review and simple impact modelling. J Volcanol Geotherm Res 158:296–306. https://doi.org/10.1016/j.jvolgeores.2006.07.002

[59] D'Addabbo M, Sulpizio R, Guidi M, Capitani G, Mantecca P, Zanchetta G (2015) Ash leachates from some recent eruptions of Mount Etna (Italy) and Popocatépetl (Mexico) volcanoes and their impact on amphibian living freshwater organisms. Biogeosciences 12:7087–7106. https://doi.org/10.5194/bg-12-7087-2015

List of Figures and Tables captions

Fig. 1 . (A) and (B) Backscattered electron (BSE) SEM images of chrysotile fiber bundles embedded in the calcite-quartz matrix of the untreated CA slates, observed on fresh fractures. (C) to (E) representative EDS spectra of chrysotile, tremolite-actinolite and crocidolite, respectively.

Fig. 2. SEM-SE (secondary electrons) images of fiber pseudomorphs after inertization. (A) and (B) low magnification images where the pseudomorphs can be easily recognized by their habitus. (C) and (D), high magnification images relating to the white boxes in (A) and (B), respectively, showing the fine grain recrystallization of the fibres. (E) and (F) representative EDS spectra of two grains with different cations abundances.

Fig. 3. Bright field (BF) TEM images (A-C) of grinded fiber pseudomorphs deposited on carbon membranes. (D) Selected area electron diffraction (SAED) pattern of olivine seen down [001]. (F) EDS spectrum of forsterite; (G) EDS spectrum of Ca-olivine; (G) EDS spectrum of glass (for explanation see text).

Fig. 4. Grain size distribution obtained through DLS after 5 (A), 10 (B), 15 (C) and 25 (D) min of milling, the last inverting the sense of rotation after 15 minutes. PM_1 size range shaded.

Fig. 5. Graphical representation of element release in solution (ppm) of the inert material and pH after 1 hour, 1 day and 2 weeks: (A) ion concentrations determined by IEC; (B) metal concentrations as determined by GFAAS.

Table 1. Bulk chemical and mineralogical compositions of the treated material. Left: EDXRF analyses (wt%). Right: XRPD quantitative phase analysis.

Table 2. DLS results.

Table 3. Leaching tests results of chemical release (ppm) of the inert material in aqueous solution after 1 hour, 1 day and two weeks. Left: IEC results of cation and anion release. Right: ICP-OES (Ni and Pb) and GFAAS (all the others) results of metal release (standard deviation in brackets; nd = not detected).

Figure 1

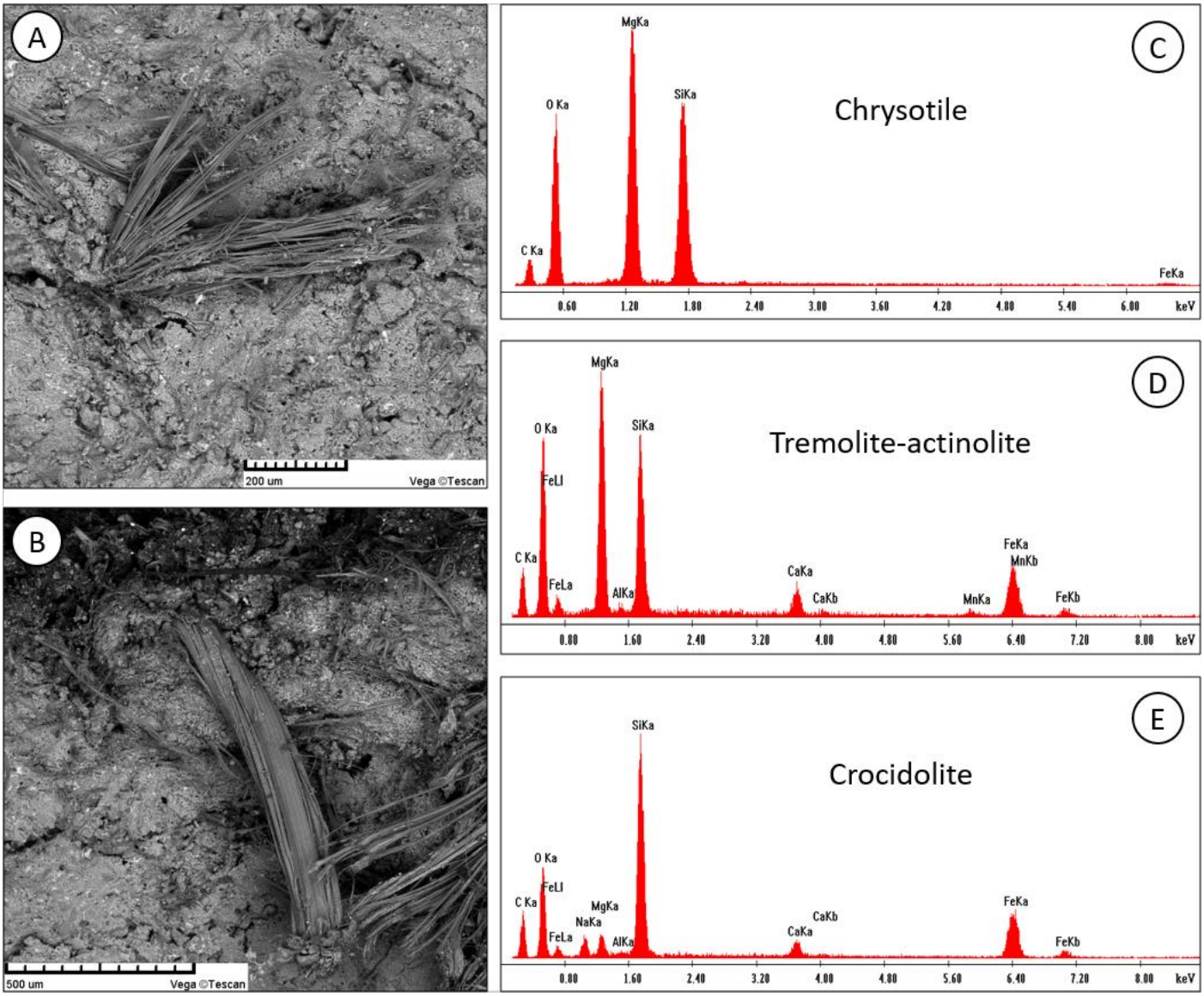

Fig. 1 . (A) and (B) Backscattered electron (BSE) SEM images of chrysotile fiber bundles embedded in the calcite-quartz matrix of the untreated CA slates, observed on fresh fractures. (C) to (E) representative EDS spectra of chrysotile, tremolite-actinolite and crocidolite, respectively.

Figure 2

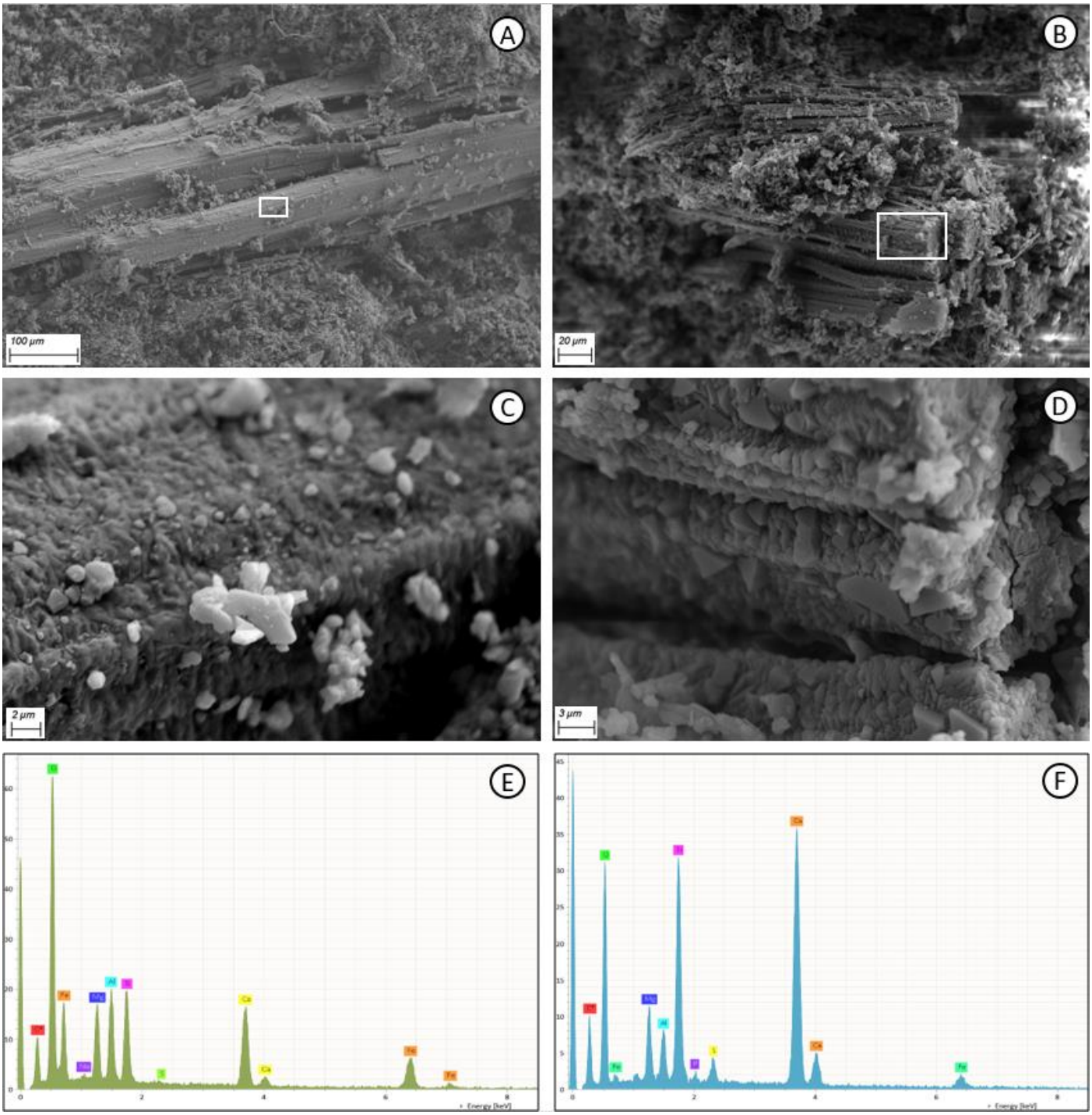

Fig. 1. SEM-SE (secondary electrons) images of fiber pseudomorphs after inertization. (A) and (B) low magnification images where the pseudomorphs can be easily recognized by their habitus. (C) and (D), high magnification images relating to the white boxes in (A) and (B), respectively, showing the fine grain recrystallization of the fibres. (E) and (F) representative EDS spectra of two grains with different cations abundances.

Figure 3

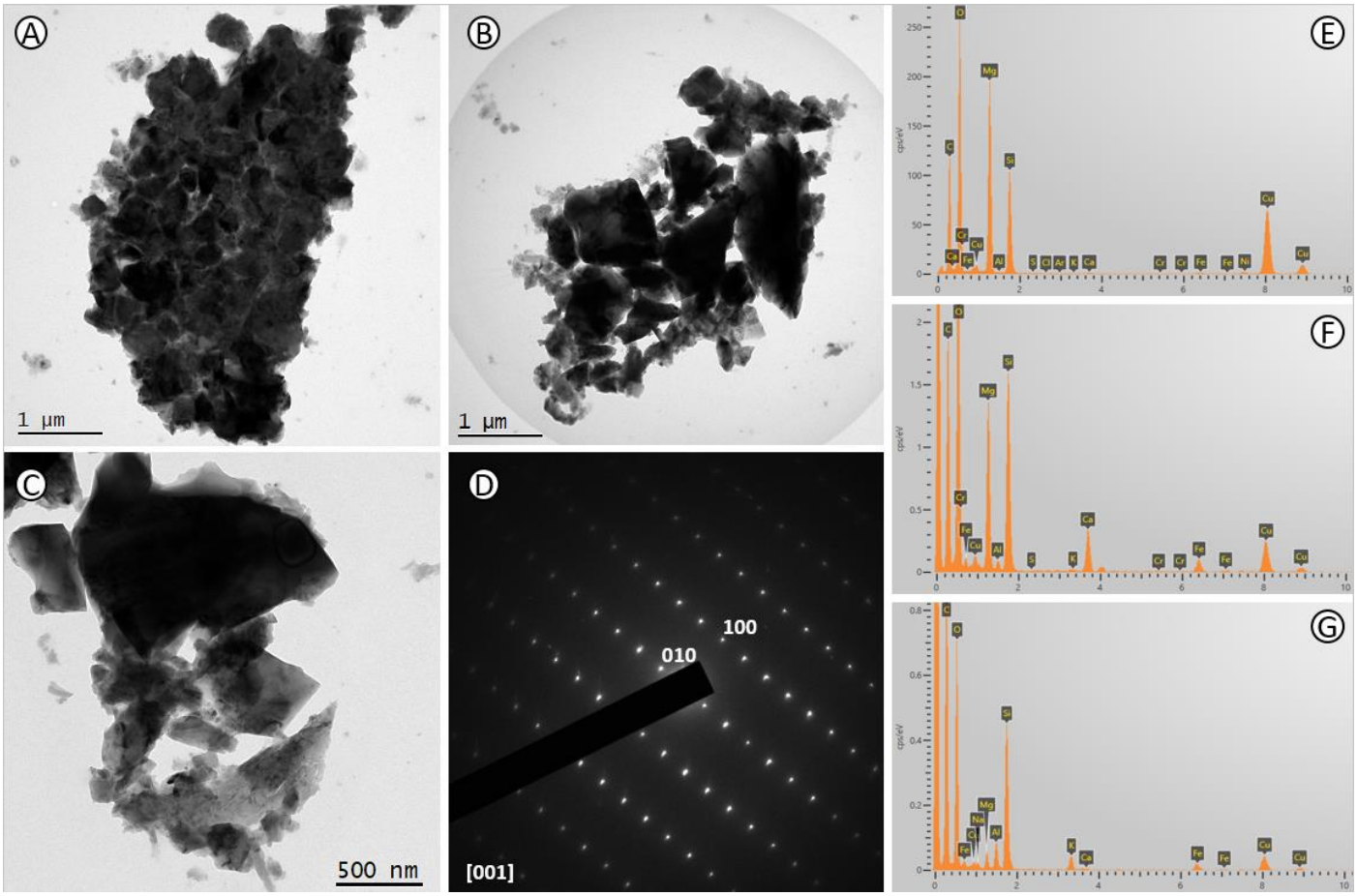

Fig. 1. Bright field (BF) TEM images (A-C) of grinded fiber pseudomorphs deposited on carbon membranes. (D) Selected area electron diffraction (SAED) pattern of olivine seen down [001]. (F) EDS spectrum of forsterite; (G) EDS spectrum of Ca-olivine; (G) EDS spectrum of glass (for explanation see text).

Figure 4

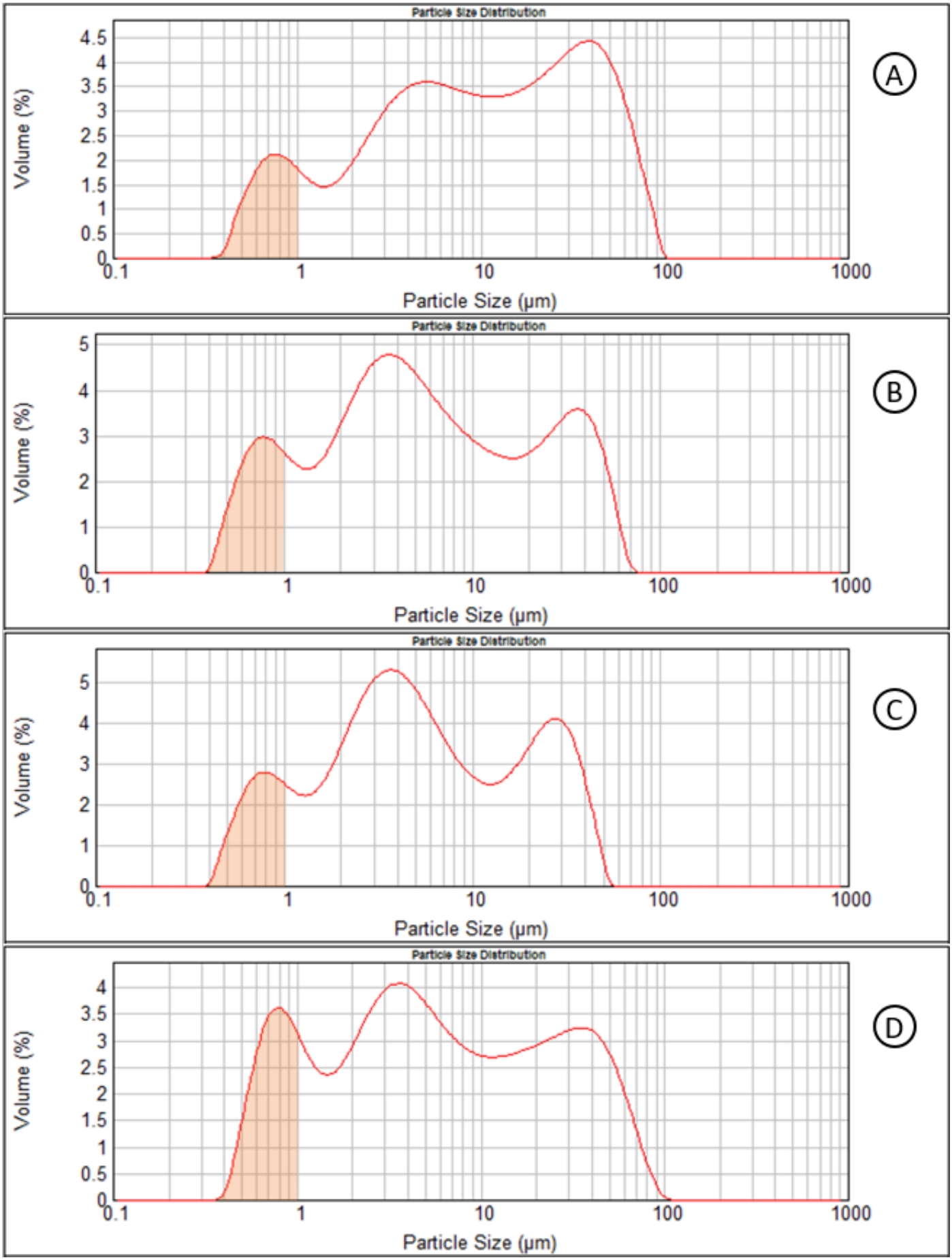

Fig. 1. Grain size distribution obtained through DLS after 5 (A), 10 (B), 15 (C) and 25 (D) min of milling, the last inverting the sense of rotation after 15 minutes. PM_1 size range shaded.

Figure 5

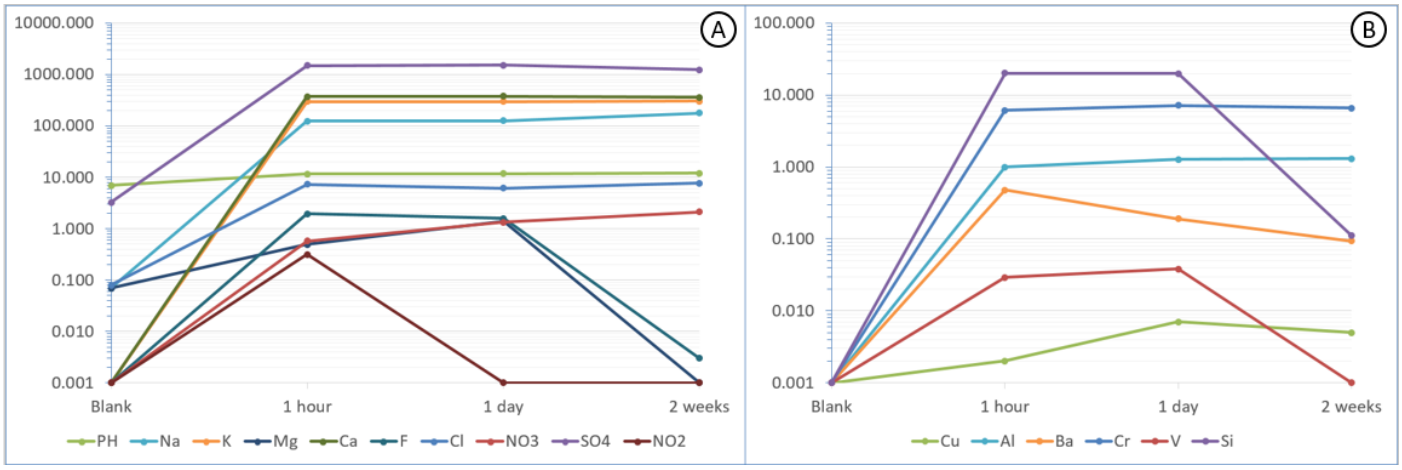

Fig. 5. Graphical representation of element release in solution (ppm) of the inert material and pH after 1 hour, 1 day and 2 weeks: (A) ion concentrations determined by IEC; (B) metal concentrations as determined by GFAAS.

Table 1

Table 1. Bulk chemical and mineralogical compositions of the treated material. Left column: EDXRF analyses (wt%). Right column: XRPD quantitative phase analysis.

Compound/wt%				**Phase**	**Chemical formula**	**Abundance (wt%)**
Na_2O	0.17	CaO	47.17	Akermanite	$Ca_2Mg(Si_2O_7)$	19.33
MgO	7.65	TiO_2	0.23	Bredigite	$Ca_{13.5}Ba_{0.3}Mg_{1.8}Mn_{0.4}Si_9O_{32}$	19.25
Al_2O_3	3.88	MnO	0.43	Merwinite	$Ca_3Mg(SiO_4)_2$	17.84
SiO_2	30.28	Fe_2O_3	5.91	Larnite	Ca_2SiO_4	3.67
SO_3	3.1	LOI	0.32	Glass		39.9
K_2O	0.42	Sum	99.56			

Table 2

Table 2. DLS results.

Milling time (min)	I max. (μm)	II max. (μm)	III max. (μm)	PM_{10} (Vol%)	$PM_{2.5}$ (Vol%)	PM_1 (Vol%)
5	39.90 – 35.56	5.64 – 5.02	0.79 – 0.70	50.11	19.96	9.42
10	3.99 – 3.55	39.90 – 35.56	0.79 – 0.70	66.23	29.35	12.56
15	3.99 – 3.55	28.25 – 25.18	0.89 – 0.80	68.37	30.52	12.57
25	3.99 – 3.55	0.79 – 0.70	35.56 – 31.70	63.01	31.31	14.80

Table 3

Table 3. Leaching tests results of chemical release (ppm) of the inert material in aqueous solution after 1 hour, 1 day and two weeks. Left column: IEC results of cation and anion release. Right column: ICP-OES (Ni and Pb) and GFAAS (all the others) results of metal release (standard deviation in brackets).

Component	**blank**	**1 h**	**1 g**	**14 g**	**Component**	**1 h**		**1 g**		**14 g**	
pH	*7.00*	11.68	11.93	12.05	Fe	*nd*		*nd*		*nd*	
Li^+	*nd*	*nd*	*nd*	*nd*	Zn	*nd*		*nd*		*nd*	
Na^+	0.072	124.566	126.295	178.252	Cu	0.0020	(4)	0.0070	(4)	0.0050	(2)
K^+	0.302	299.395	296.329	301.581	Mn	*nd*		*nd*		*nd*	
Mg^{2+}	*nd*	0.498	1.401	*Nd*	Al	0.9950	(789)	1.2700	(718)	1.3090	(166)
Ca^{2+}	*nd*	371.838	377.266	359.585	Ba	0.4780	(87)	0.1910	(46)	0.0940	(35)
F^-	*nd*	1.946	1.59	0.003	Cr	6.1150	(220)	7.2290	(699)	6.6380	(471)
Cl^-	0.078	7.338	6.128	7.769	Ti	*nd*		*nd*		*nd*	
Br^-	*nd*	*nd*	*nd*	*nd*	V	0.0290	(5)	0.0380	(30)	*nd*	
NO_3^{2-}	nd	0.578	1.341	2.139	Sn	nd		nd		*nd*	
SO_4^{2-}	3.252	1491.818	1533.766	1236.869	Si	20.1000	(1250)	20.0200	(1790)	0.1110	(5620)
PO_4^{3-}	*nd*	*nd*	*nd*	*nd*	Ni	*nd*		*nd*		*nd*	
NO_2^-	*nd*	0.314	*nd*	*nd*	Pb	*nd*		*nd*		*nd*	